International Journal of Heat and Mass Transfer 52 (2009) 2427–2436

Contents lists available at ScienceDirect

International Journal of Heat and Mass Transfer

journal homepage: www.elsevier.com/locate/ijhmt

Confinement effects on nucleate boiling and critical heat flux in buoyancy-driven microchannels

K.J.L. Geisler [a,*], A. Bar-Cohen [b]

[a] General Dynamics Advanced Information Systems, 8800 Queen Avenue South, Bloomington, MN 55431, USA
[b] University of Maryland, Department of Mechanical Engineering, College Park, MD 20742, USA

ARTICLE INFO

Article history:
Received 1 January 2008
Received in revised form 13 January 2009
Available online 28 February 2009

Keywords:
Boiling
Microchannel
Confinement
Electronics cooling
Heat transfer

ABSTRACT

Pool boiling and CHF experiments were performed for vertical, rectangular parallel-plate channels immersed in the dielectric liquid FC-72 at atmospheric pressure to elucidate the effects of geometrical confinement in immersion cooled electronics applications. Heat transfer enhancement in the low flux region of the nucleate boiling curve was observed for channel spacings near and below expected bubble departure diameters, but was widely different for two different heater materials. Relative degradation of CHF with decreasing channel spacing was found to be a strong function of channel aspect ratio and independent of surface material and finish.

1. Introduction

In light of continually increasing performance demands, direct liquid cooling of high heat flux electronic components remains a leading option for future thermal packaging solutions. As a result, many researchers have considered exploiting the high heat transfer rates of nucleate boiling for immersion cooling, with particular attention paid to predicting and extending the pool boiling critical heat flux (CHF) limit [1]. Complexities inherent to the boiling process (nucleation site characteristics, interfacial stability, two phase flow, etc.) make the prediction of boiling heat transfer rates and CHF significantly more complicated and significantly less accurate than comparable single phase calculations. Due to ongoing microsystem miniaturization, the effects of physical confinement in electronic systems further complicate the heat transfer processes involved and may ultimately lead to deteriorated performance relative to unconfined pool boiling.

Confined boiling occurs in a variety of applications, including cryogenics [2], nuclear reactor cooling [3], shell and tube heat exchangers [4], and steam power generation [5]. As a result, it has garnered considerable attention over the past half century. Ishibashi and Nishikawa [6] explored relative effects of confinement on saturated water and alcohol boiling in narrow vertical annuli, under natural circulation conditions. Since this landmark study, numerous researchers have explored boiling heat transfer in parallel-plate channels, tubes, and other confined geometries.

Table 1 presents a representative summary of studies of natural convection boiling in vertically-oriented parallel-plate channels. General observations may be summarized as follows: at channel spacings that are large compared to the size of generated vapor bubbles and when channel aspect ratio (height divided by spacing) is less than 10, boiling behavior proceeds as in unconfined pool boiling. When the channel aspect ratio is larger than 10, increasing vapor fractions in the channel lead to premature dry out at the heated surface(s), beginning at or near the channel exit. When the channel spacing is reduced below the bubble departure diameter, heat transfer enhancement is often seen in the low heat flux region of the nucleate boiling curve. Enhancement in the low heat flux region continues to increase with decreasing channel spacing until reaching a maximum, after which further reductions in channel spacing lead to reduced enhancement and, subsequently, deteriorated heat transfer across the entire boiling curve.

The observations that the majority of the studies summarized in Table 1 employed saturated water or R-113 as the working fluid and nearly all channels consisted of a single heated copper wall and an opposing adiabatic wall (asymmetric heating) further exacerbate the applicability of this body of research to immersion cooling of electronic devices. As nucleate boiling is highly dependent on surface conditions, phenomena observed on metallic surfaces may not be relevant to silicon or other common microelectronic device materials. The saturation temperature of water near atmospheric pressure puts surface temperatures during nucleate boiling well in excess of typical integrated circuit operating requirements, and the thermophysical properties of water are vastly different from those of more suitable electronics cooling liquids.

* Corresponding author. Tel.: +1 952 921 6575; fax: +1 952 921 6345.
E-mail address: karl.geisler@gd-ais.com (K.J.L. Geisler).

0017-9310/$ - see front matter © 2009 Elsevier Ltd. All rights reserved.
doi:10.1016/j.ijheatmasstransfer.2009.02.001

Nomenclature

Bo	Bond number
c_p	specific heat (J/kg K)
D_b	bubble diameter (m)
g	gravitational acceleration (m/s^2)
h	heat transfer coefficient (W/m^2 K)
h_{fg}	latent heat of vaporization (J/kg)
Ja′	modified Jakob number
K	thermal conductivity (W/m K)
L	channel height, length in primary flow direction (m)
M	molecular weight (g/mol)
P	pressure (Pa)
P_r	reduced pressure, P/P_{crit}
q''	heat flux (W/m^2)
R_p	RMS surface roughness (μm)
T	temperature (°C)
t	heater thickness (m)
Greek	
δ	channel spacing (m)
ρ	density (kg/m^3)
σ	surface tension (kg/s^2)
Subscripts	
CHF	critical heat flux
crit	critical
f	liquid phase
g	vapor phase
h	heater
sub	subcooling

In many potential immersion cooling configurations, such as boiling heat sinks [15] or stacked dies [16], symmetric heating conditions would be expected. Most of the channels represented in the literature are many times longer in the vertical (flow) direction than typical microelectronic components (<30 mm). In addition, most of the channels studied were many times longer than they were deep, potentially resulting in significant edge effects and an exaggerated importance of side periphery conditions.

Thus, in order to address these questions of applicability and evaluate confined boiling correlations for electronics cooling applications, an experimental system was constructed to facilitate the investigation of pool boiling heat transfer in various parallel-plate channels, focusing on sub-millimeter spacings. Experiments were conducted for the dielectric liquid FC-72 boiling, at atmospheric pressure, from silicon (20 mm × 20 mm and 20 mm × 30 mm) and aluminum (20 mm × 20 mm) heaters, respectively, with varying surface roughness. Channel spacing was varied from 20 mm to 0.3 mm, providing channel aspect ratios (height/spacing) from effectively zero to 67. Experiments were performed with uniform, equal heat flux on both channel walls (symmetric heating), as well as with one side heated and the other adiabatic (asymmetric heating).

2. Experimental system

2.1. Experimental module

Fig. 1 shows two views of the experimental module which was formed from a 102 × 140 × 44 mm aluminum block. An 80 mm square hole was machined through the thickness of the block to accommodate the liquid volume. The enclosure is completed by 108 mm square by 6 mm thick polycarbonate walls secured to the module with machine screws and sealed with o-ring gaskets. These transparent walls serve as the mounting surfaces for the various heater assemblies used in the experiments. The configuration shown in Fig. 1a has a single, stationary 20 mm × 30 mm silicon heater mounted in the center of the rear polycarbonate wall.

Four 8 mm diameter water channels, two passing through each end of the aluminum module, receive heated water to maintain the temperature of the module at the 56.6 °C saturation temperature of FC-72 at 1 atm. Four 1.6 mm sheath diameter bulk liquid thermocouples pass through the end of the module via Swagelok® pipe fittings with Teflon® ferrules to allow for positioning and subsequent repositioning within the module. Fluid sampling and drainage ports were located in the bottom of the module to facilitate filling and draining the module and dissolved gas content measurements, as shown in Fig. 1a. Dissolved gas content was measured using a Seaton-Wilson Aire-Ometer (model AD-4003) air measuring instrument. The FC-72 liquid was degassed to well below 4% by volume by increasing the temperature of the module control water above the saturation temperature and applying power to the heaters to stimulate intense bubble formation and transport of the vapor and air into the vapor space at the top of the module. In order to minimize vapor loss (both during degassing as well as normal operation), the generated vapor was directed to two 300 mm, water cooled Allihn condensers connected to nylon pipe fittings installed in the top of the module through 150 mm long sections of 19 mm inner diameter Tygon® C-544-A I.B. hose. Fig. 1b shows the condensers, as well as an adjustable heater positioning shaft installed in the front module wall (discussed in the next section). Further details of the experimental apparatus, schematics, and additional photographs appear in [17].

Table 1
Summary of representative studies of natural convection boiling in vertical channels.

Study	Fluid(s)	Heater surface material	Sym./ Asym.[a]	Channel length (mm)	Channel depth (mm)	Channel spacing (mm)	Peripheral boundary
[7]	Water ethanol R-113 benzene	Copper	A	20, 35, 50	10	0.45–7.0	All open
[8]	Water	Copper	A, S	240	66	2–20	Closed sides
[9,10]	Water	Copper	A	30, 120	30	0.15–5	Open all, closed sides and bottom
[11]	R-113	Semi-conductive oxide	S	56, 88, 128, 197	45	0.8–5	Open all, closed sides
[2]	Helium	Copper	A	150, 220	35	0.4–1.5	Closed sides
[12,13]	R-113	Copper	A	50, 120	20, 60	0.3–2.5	All open
[14]	Methanol HFC4310	Copper	A	55 mm diameter circular disk		1, 2, 25	All open

[a] Relates to heating condition: symmetric = both channel walls heated, asymmetric = one heated, one adiabatic.

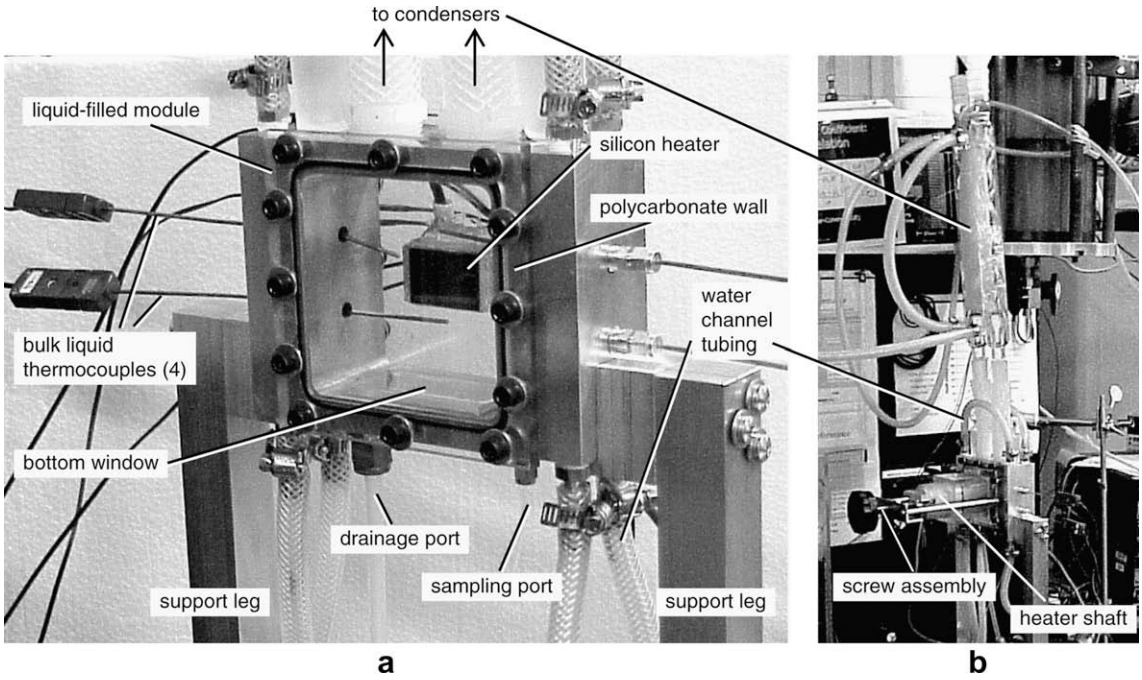

Fig. 1. The experimental module.

2.2. Silicon heaters

Silicon heaters were fabricated using a 0.675 mm thick, double-side polished, doped silicon wafer with an electrical resistivity of 0.012 Ω m. In order to provide electrical contact, 10 μm thick aluminum layers were deposited on opposing 20 mm edges via DC sputtering. The silicon heaters were mounted on polycarbonate substrates with quick-setting epoxy. Fig. 2 shows a photograph of a 20 mm × 20 mm silicon heater and substrate mounted on a module wall. Small substrate pockets, approximately 1 mm in from each heater edge, were machined into the polycarbonate substrates in the area below the heaters to minimize parasitic heat losses and accommodate attachment of a thin foil thermocouple to the center of the backside of the silicon with thermally conductive epoxy. Electrical contact is made between the edges of the silicon and pairs of 0.3 mm thick brass electrodes through electrically conductive silver epoxy. Exposed edges of the heaters and brass electrodes are covered with quick-setting epoxy to restrict heat loss from the edges and to prevent fluid penetration behind the heater. The brass electrodes pass through the back of the polycarbonate substrates for connection to a DC power supply with 12-gauge copper wire fitted with screw terminal lugs. Sensing leads, for heater voltage measurement, are soldered to the brass electrodes. Foil thermocouple leads are covered with heat-shrink tubing for mechanical support and to prevent shorting (Fig. 2).

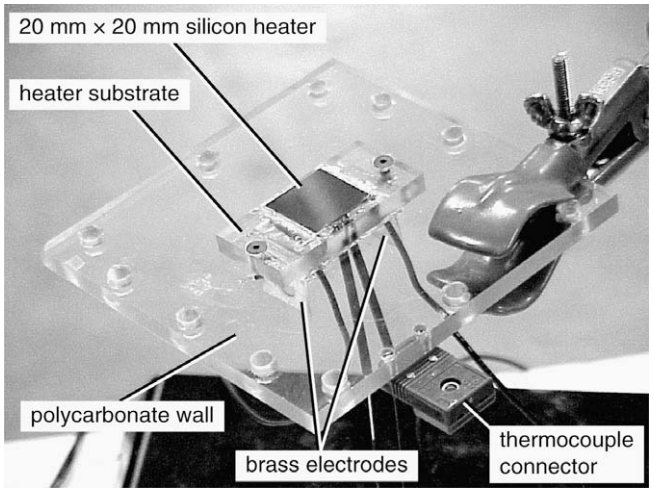

Fig. 2. A 20 mm × 20 mm silicon heater assembly mounted on a module wall.

To create the desired parallel-plate channels, heaters are attached directly to the rear module wall (as in Fig. 1a) and to the end of the positioning shaft (shown in Fig. 1b). The 102 mm long, 51 mm diameter cylindrical polycarbonate shaft passes through a 64 mm square block mounted on the outside of the front module wall. A pair of o-ring grooves and gaskets, located in the middle of the shaft, maintains a liquid seal. A screw assembly facilitates precise positioning of the shaft to create parallel-plate channels with variable spacing, δ. Channel spacings are calculated from measurements of the shaft position. Reported channel spacings are estimated to be accurate within ±0.1 mm, based on numerous measurements from various module reference surfaces as well as digital photographs of the interior of the module taken through an observation window located on its bottom side (Fig. 1a). Each heater, or channel wall, is powered separately.

2.3. Aluminum heaters

Aluminum heater assemblies were fabricated via electrical discharge machining (EDM). Fig. 3 shows the heater assembly, which consists of two sections. The boiling surface portion of the assembly (Fig. 3a) consisted of a 20 mm × 20 mm × 10 mm block of aluminum with a pair of short flanges for attachment to the heater section (Fig. 3b). The boiling surface and heater sections are held together with 4–40 machine screws. Heat is supplied by a 9.5 mm diameter, 31.8 mm long, 39 Ω cartridge heater fit snugly into a deep hole in the heater section. Thermally conductive grease was applied to the surface of the cartridge heater as well as the interface between the boiling surface and heater sections. A thin foil thermocouple was attached to the side of the assembly with

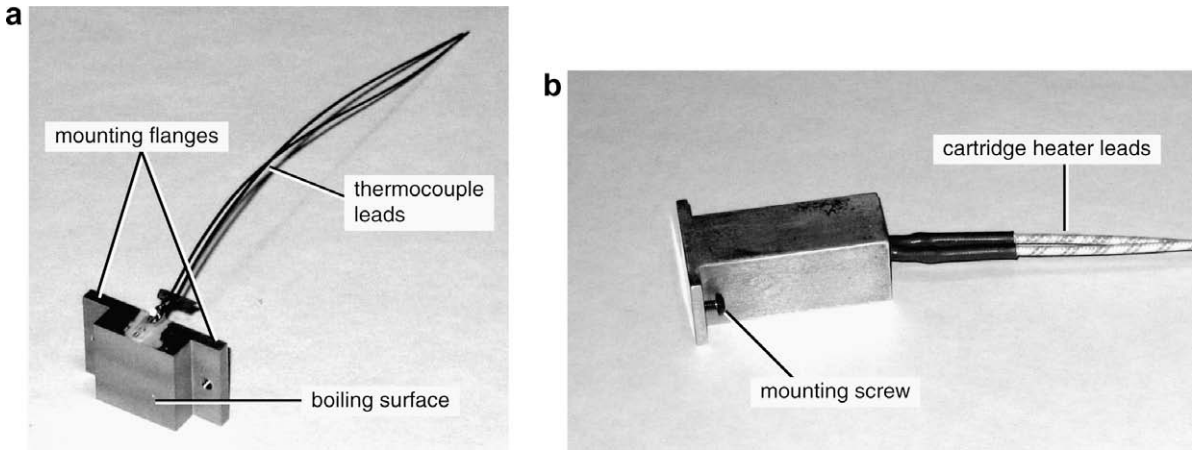

Fig. 3. Aluminum heater assembly parts: (a) boiling surface (matte EDM finish) with attached foil thermocouple, and (b) cartridge heater section.

thermally conductive epoxy, with the sensing tip within 1 mm of the boiling surface. The aluminum heater assembly was epoxied into a 20 mm × 20 mm square opening in the polycarbonate module wall so that the boiling surface is flush with the interior wall surface. In addition to providing a method of attachment for the heater section, the bolt flanges also assist in alignment of the boiling surface.

Due to the physical size of the aluminum heater assembly and constraints of the shaft geometry, the aluminum heater experiments are limited to asymmetric heating. Channels were formed between the single fixed boiling surface described above and a 20 mm high by 30 mm wide piece of polycarbonate. The distance from the boiling surface to the unheated polycarbonate channel wall was set by multiple layers of polyimide tape serving as "spacers" at the sides. This arrangement was also used for some of the asymmetric silicon channel experiments. Identical experimental results for asymmetric silicon channels in saturated liquid were obtained when using this polycarbonate plate or a shaft-mounted unheated silicon heater as the opposing channel wall. Consequently, experiments using the polycarbonate wall provide an additional means of validating the accuracy of shaft position and silicon channel spacing measurements.

2.4. Boiling surface conditions

The original silicon and aluminum heater surfaces were modified to examine the effect of surface finish. The magnified photographs of Fig. 4a show the relatively rough and pitted surface of the EDM aluminum heater. The aluminum surface was subsequently polished in two stages. First, the aluminum was sanded with 400 grit sandpaper. Secondly, a wet 600 grit paper was used to obtain an even smoother appearance, shown in Fig. 4b. While surface roughness was not measured directly, as will be discussed in Section 3.1, the effective surface roughness of the EDM, 400 grit, and 600 grit aluminum surfaces are estimated to be 20, 4.5, and 2.5 μm, respectively. The original polished silicon surface was roughened with 60 grit sandpaper to a cloudy appearance, shown in Fig. 4c.

2.5. Experimental procedure

Dissolved gas content measurements were taken at the beginning and end of each experiment. Heater shaft location was measured multiple times throughout the course of each channel experiment. Power supplies and digital voltmeters were accessed through GPIB interfaces by a Pentium-class computer running the Linux operating system. Data acquisition and reduction was automated through the use of a custom C language program. The automated acquisition system obtained a complete set of readings every 3 to 4 s. The output file created by the data acquisition program contains raw voltage measurements as well as various derived quantities (temperature, heater current, power, and resistance).

In addition to displaying measurement data in text format at the end of each cycle, the data acquisition program also launches the Gnuplot plotting program for real-time graphical display of the output file. The graphs facilitate identification of when steady-state conditions have been reached for each power setting. After reaching steady-state, the data acquisition program was allowed to cycle through more than 30 additional sets of readings to capture a statistically significant sample of data before moving to the next power setting.

Voltage settings on the primary power supply were controlled manually, but keyboard commands were implemented in the data acquisition program to assist in control of the experimental process. Control of the power supply feeding the secondary heater may be toggled between manual and automatic control. During automatic control, the data acquisition program adjusts the secondary power supply to match the power dissipation of the primary power supply. Power to either or both heaters may be terminated manually via keyboard commands. In the event that the data acquisition program measures a heater temperature exceeding 100 °C, signaling CHF and a transition to film boiling, power is cut automatically while data acquisition continues. No damage to the heaters was observed after these brief film boiling events. Additional details of the experimental system are provided in [17].

2.6. Experimental uncertainties

As most of the aluminum heater assembly was external to the module, the exposed heater section was covered with two layers of 6.4 mm thick polyethylene foam insulation. Parasitic heat losses were evaluated for all heaters through CFD analyses of the exterior of the liquid-filled module, as presented in [17]. Percentage heat loss is estimated to be greatest at low flux and decreases asymptotically as CHF is approached. From early nucleate boiling to CHF, heat loss estimates range from 10% to 2% and 30% to 10% for the silicon and aluminum heaters, respectively. Heat flux values for the silicon heaters were also cor-

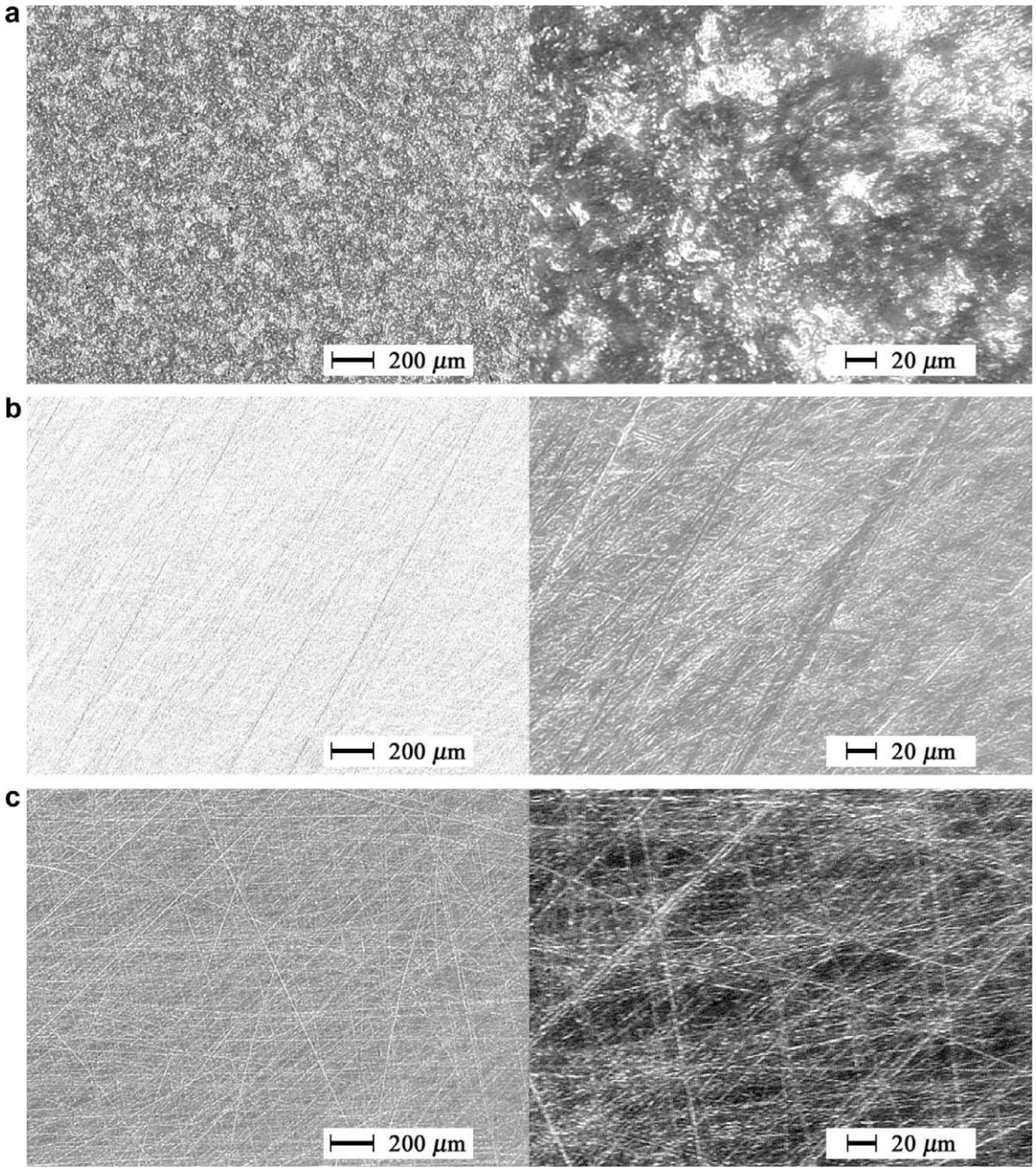

Fig. 4. Magnified images of heater surfaces: (a) aluminum surface formed by wire EDM process (b) aluminum surface after treatment with 600 grit sandpaper (c) scratched silicon surface.

rected to account for small areas at the heater edges where epoxy covered and insulated a small portion (<6%) of the boiling surface. Heat flux uncertainty estimates are ±3% of reported values for all heaters. The majority of this uncertainty is from the parasitic heat loss correction, with the remainder primarily attributable to shunt resistor voltage (heater current) fluctuations. Primary measurements, their ranges, and their estimated uncertainties at the 95% confidence level, for the 40 distinct experimental cases, are

- Temperature: 20–100 °C ± 0.6 °C absolute, ±0.4 °C difference.
- Boiling heat flux: 5–160 kW/m^2 ±3%.
- Channel spacing: 0.3–20 mm ±0.1 mm.

3. Experimental results

3.1. Unconfined pool boiling

Saturated pool boiling data obtained at atmospheric pressure are shown in Fig. 5 for a large heater separation (channel spacing) of approximately 20 mm. The leftmost curve in Fig. 5 represents boiling data obtained for the aluminum heater with the EDM surface, while the rightmost is polished silicon. All low flux data shown were obtained with decreasing heat flux. High flux data obtained with increasing and decreasing heat flux were indistinguishable.

In the fully-developed nucleate boiling region, the polished silicon surface achieved boiling heat transfer coefficients ranging

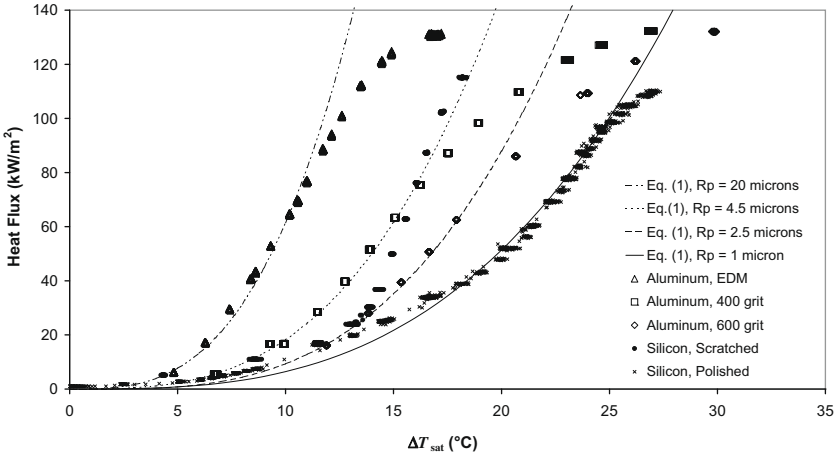

Fig. 5. Unconfined pool boiling curves for various aluminum and silicon surfaces compared to Cooper correlation, Eq. (1).

from 2 to 4 kW/m^2 K. The rough and pitted EDM aluminum surface provides significantly better heat transfer performance at comparable superheats and heat transfer coefficients in excess of 9 kW/m^2 K. Nucleate boiling heat transfer coefficients for the modified silicon and aluminum surfaces ranged from 2 to 6 kW/m^2 K.

Cooper [18] developed the following empirical pool boiling heat transfer correlation based on three fluid and surface properties:

$$h_b = (55P_r^{0.12-0.2\log_{10}R_p}(-\log_{10}P_r)^{-0.55}M^{-0.5})^3\Delta T^2 \quad (1)$$

P_r is the reduced system pressure (P/P_{crit}), M is the molecular weight of the fluid (g/mol), and R_p is the RMS surface roughness in microns (μm). Reduced pressure is employed to represent the dominant property variations of a given fluid, while molecular weight was shown to capture the general behavior of multi-property correlations evaluated for a variety of fluids [18]. The surface roughness factor is based on one suggested by Nishikawa et al. [19] and includes the observed trend that boiling is more dependent on roughness at low reduced pressure than at high reduced pressure. Eq. (1) suggests that the dominant effect leading to different boiling heat transfer coefficients for different surfaces is the surface roughness.

Pool boiling predictions based on Eq. (1) for FC-72 at atmospheric pressure and a variety of surface roughnesses are included in Fig. 5. Experimental data for the rough EDM aluminum surface are shown to be well represented by Eq. (1) with a surface roughness of 20 μm. Likewise, the effective Nishikawa roughnesses of the 400 grit and 600 grit aluminum surfaces are found to equal 4.5 and 2.5 μm, respectively. While the fully-developed nucleate boiling portion of the polished silicon data matches Eq. (1) with a surface roughness of 1 μm, the scratched silicon surface data varies between predictions for R_p equal to 2 μm at low flux to 5 μm at high flux. Clearly, while it is impossible to accurately represent the nucleation site characteristics of vastly different surfaces with a single number, the data support the general trend of increased heat transfer with increased surface roughness.

The highest heat flux data shown in Fig. 5 suggests that surface treatment does not have a significant effect on CHF. However, a clear difference in CHF was observed between the aluminum and silicon heaters, 137 vs. 114 kW/m^2, respectively, averaged over all unconfined saturated boiling experiments.

3.2. Channel boiling

Figs. 6 and 7 show decreasing-flux boiling curves for symmetrically and asymmetrically heated polished silicon channels, respectively. Each symbol in these graphs represents an average of at least 30 data points. As channel spacing is decreased below

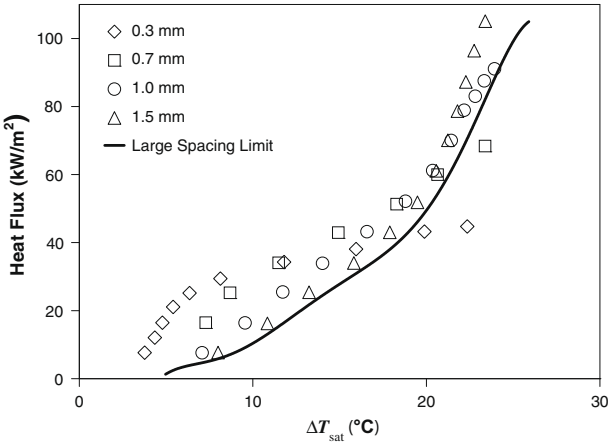

Fig. 6. Boiling curves for symmetric 20 × 30 mm polished silicon heater channels.

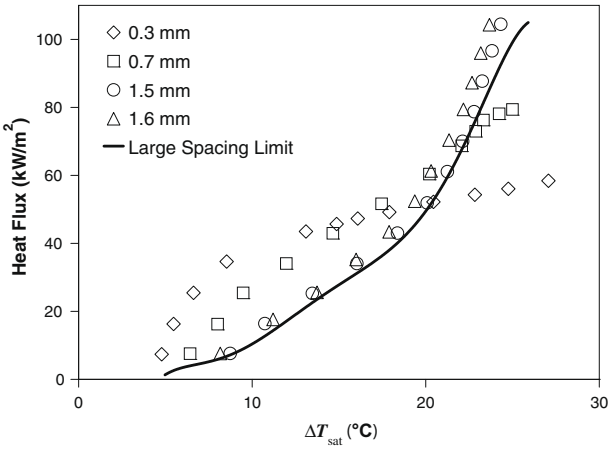

Fig. 7. Boiling curves for asymmetric 20 × 30 mm polished silicon heater channels.

2 mm, and the heated surfaces begin to interact, the boiling curves shift slightly to the left, signifying subtly enhanced heat transfer. With further decreases in channel spacing, heat transfer at low heat fluxes is greatly enhanced, while CHF values and boiling data in the high flux region show deteriorated performance.

At heat fluxes ranging from 40 to 60 kW/m^2 for symmetrically heated channels and 50 to 70 kW/m^2 for asymmetrically heated

channels, boiling surface temperatures increase beyond those observed for unconfined pool boiling, as seen in Figs. 6 and 7, signifying a transition to deteriorated heat transfer performance with channel confinement. CHF was observed to decrease with reduced channel spacing, at a greater rate for symmetric channels than asymmetric channels of the same spacing. The observation that channel spacing effects are more pronounced for symmetric channels is expected, since at a given heat flux twice as much heat is being transferred from the combined (double) surface area of both channel walls in the symmetric configuration.

4. CHF correlation

4.1. Unconfined pool boiling

The well known Kutateladze–Zuber CHF correlation [20] was developed for saturated pool boiling on large, thick, upward-facing horizontal plates.

$$q''_{CHF} = \frac{\pi}{24} h_{fg} \sqrt{\rho_g} \left[\sigma_f g (\rho_f - \rho_g) \right]^{1/4} \tag{2}$$

The Zuber analytical treatment considered the Taylor instability criterion for vapor columns formed by coalesced bubbles and defined CHF as the heat flux at which the vapor–liquid interface becomes unstable. More recent research has suggested that, for horizontal heaters, lateral bubble coalescence creates dry patches on the surface that eventually reach the Leidenfrost temperature and trigger CHF [21]. Mudawar et al. [22] derived an interfacial lift-off model for CHF on vertical surfaces based on an analysis of Kelvin–Helmholtz waves. Their resulting equation is identical in form to Eq. (2), despite being based on a different assumed mechanism. Regardless of its derivation, Eq. (2) remains relatively accurate and, in particular, captures the effect of system pressure on CHF. CHF for the Fluorinert™ liquids as predicted by Eq. (2) is typically in the range of 100–200 kW/m^2.

Arik and Bar-Cohen [21] expanded the Kutateladze–Zuber correlation to incorporate a wide variety of parametric effects. Using relations from the literature [23–25], their correlation modifies Eq. (2) by parametric factors which take into account effects of heater characteristics and bulk liquid subcooling:

$$q''_{CHF} = \frac{\pi}{24} h_{fg} \sqrt{\rho_g} \left[\sigma_f g (\rho_f - \rho_g) \right]^{1/4} \left(\frac{t \sqrt{\rho_h c_{p,h} k_h}}{t \sqrt{\rho_h c_{p,h} k_h} + 0.1} \right) \cdot (1 + \langle 0.3014 - 0.01507 L \prime \rangle) \left\{ 1 + 0.03 \left[\left(\frac{\rho_f}{\rho_g} \right)^{0.75} \frac{c_{p,f}}{h_{fg}} \right] \Delta T_{sub} \right\} \tag{3}$$

where

$$L' = L \sqrt{\frac{g(\rho_f - \rho_g)}{\sigma_f}}$$

The quantity $\langle 0.3014–0.01507L' \rangle$ in Eq. (3) reflects the increase in CHF observed for small heaters. It is included only when positive, corresponding to heater lengths below approximately 14 mm for FC-72 at atmospheric pressure. The effusivity factor appearing in Eq. (3) is based on heater thickness, density, specific heat, and thermal conductivity. Silicon properties typically put traditional microelectronic IC devices in the "thick heater" domain. CHF for a 130 μm thick silicon heater would be within 5% of the asymptotic limit, while the 5% thickness for an aluminum surface would be 175 μm. For the 675 μm silicon and greater than 10 mm thick aluminum heaters employed in this study, the effusivity factor is found to equal 0.990 and 0.9995, respectively. The final factor in Eq. (3) captures the enhancement effect of liquid subcooling on CHF.

For saturated pool boiling CHF of FC-72 at atmospheric pressure, Eq. (3) predicts a CHF of 137 kW/m^2 for the thick aluminum heaters—identical to the experimental result. The CHF difference observed between the aluminum and silicon heater experiments, 137 vs. 114 kW/m^2, can not be explained by any of the parametric effects included in Eq. (3) or the estimated experimental uncertainty of ±3%. As noted above, effusivity effects for the 0.675 mm thick silicon would be expected to decrease CHF values by less than 1% relative to that achieved by a thick aluminum plate. However, all unconfined CHF values are well within the correlation accuracy of Eq. (3) as stated by Arik and Bar-Cohen [21], ±25% at 95% confidence. The reader is reminded that the focus of this work is the deleterious effects of confinement on CHF, and regardless of the source of this discrepancy, channel CHF will be evaluated relative to the unconfined data observed for each type of surface.

Subcooled CHF data were obtained for 20 mm × 20 mm polished silicon heaters. Because the module was open to the atmosphere, it was not possible to have the liquid both subcooled and degassed simultaneously. Thus, bulk liquid in the subcooled experiments contained approximately 30% gas (by volume). CHF for the silicon heaters increased with subcooling, from 114 kW/m^2 at saturated conditions to 126 kW/m^2, 147 kW/m^2, and 162 kW/m^2 with 10 °C, 19 °C, and 32 °C of subcooling, respectively. Enhancement of CHF with subcooling may be considered in isolation by extracting the subcooling factor of Eq. (3) [25], i.e.

$$\frac{q''_{CHF,Subcooled}}{q''_{CHF,Saturated}} = 1 + 0.03 \left[\left(\frac{\rho_f}{\rho_g} \right)^{0.75} \frac{c_{p,f}}{h_{fg}} \right] \Delta T_{sub} \tag{4}$$

Enhancement of CHF with subcooling observed in the present data is correlated very well by Eq. (4), within the previously-stated temperature and heat flux experimental uncertainties included as error bars on the data points shown in Fig. 8.

4.2. Channel CHF correlation

Bonjour and Lallemand [12], expanding on the work of Monde et al. [7], explored CHF of R-113 in asymmetrically heated channels over a pressure range of 100–300 kPa and channel aspect ratios approaching 170. In order to account for observed pressure effects, Bonjour and Lallemand [12], following the form of an equation proposed by Monde et al. [7] with an additional term based on the reduced pressure, presented a correlation for CHF in asymmetrically heated, narrow vertical channels.

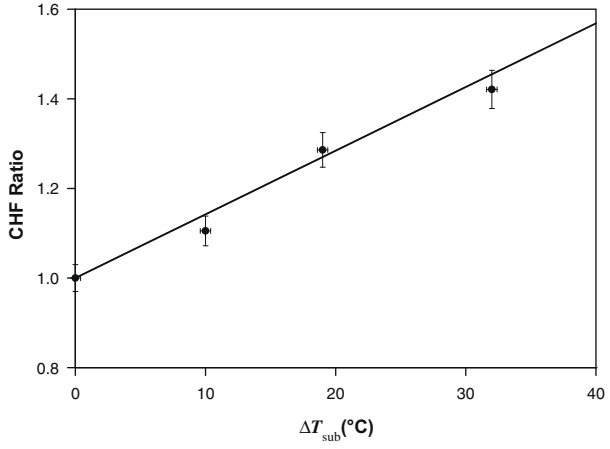

Fig. 8. Subcooling enhancement of CHF for unconfined polished silicon heaters.

$$\frac{q''_{CHF}}{q''_{(L/\delta=0)}} = \left[1 + 6.39\times10^{-5}\left(\frac{\rho_f}{\rho_g}\right)^{\Psi}\left(\frac{L}{\delta}\right)^{1.517}\right]^{-1} \quad (5)$$

where

$$\Psi = 1.343P_r^{0.252}$$

This equation agrees with their own data to within ±5% and that considered by Monde et al. [7] for ethanol, R-113, and Benzene to within ±12%. In addition to the channel spacing/aspect ratio trends observed by Monde et al. [7], Bonjour and Lallemand [12] observed an increase in CHF with increasing pressure, though at a decreasing rate as the channel spacing narrows.

CHF data obtained in the current study were normalized by the average CHF observed for each heater material at large channel spacings ($L/\delta < 5$) and are shown in Fig. 9. All surfaces display the same decreasing CHF behavior with decreasing channel spacing. For the most part, the asymmetric channel data shown in Fig. 9 agree with the Bonjour and Lallemand [12] correlation within its stated accuracy of ±12%. There are a few outliers, particularly at high aspect ratio. However, given the channel spacing measurement uncertainty of ±0.1 mm, a channel aspect of ratio of 67 (δ = 0.3 mm) could represent an actual spacing ranging from 50 to 100. The horizontal error bars included in Fig. 9 represent this uncertainty.

As previously discussed, the effect of channel spacing on CHF is stronger for symmetrically heated channels, and Eq. (5) does not apply. As a first-order attempt to correlate symmetric channel CHF data, the aspect ratio (L/δ) in the asymmetric correlation is multiplied by the square root of two. The resulting channel CHF correlation analogous to Eq. (5) but for symmetrically heated channels is then

$$\frac{q''_{CHF}}{q''_{(L/\delta=0)}} = \left[1 + 1.08\times10^{-4}\left(\frac{\rho_f}{\rho_g}\right)^{\Psi}\left(\frac{L}{\delta}\right)^{1.517}\right]^{-1} \quad (6)$$

where the 6.39×10^{-5} coefficient in Eq. (5) has been multiplied by a factor of $(\sqrt{2})^{1.517}$ from the aspect ratio factor. Fig. 10 shows that Eq. (6) comes well within ±12% of the symmetric channel CHF data.

5. Discussion

5.1. Low flux enhancement

As discussed in the introduction, low flux confinement effects tend to be primarily driven by the relationship of the channel spacing, δ, to the bubble departure diameter, D_b. Tong et al. [26] explored the suitability of a variety of bubble correlations for highly-wetting liquids, including FC-72. They determined that the Cole and Rohsenow [27] departure diameter model best fit available experimental data:

$$D_b = \sqrt{\frac{\sigma_h E}{g(\rho_f - \rho_g)}} \quad (7)$$

where

$$E = (0.000465\cdot \mathrm{Ja}'^{5/4})^2$$

and

$$\mathrm{Ja}' = \frac{c_p\rho_f T_{sat}}{\rho_g h_{fg}}$$

with the saturation temperature specified in absolute degrees. Tong et al. [26] modified the Cole and Rohsenow [27] correlation to include the heater temperature dependence of departure diameter by evaluating the surface tension in Eq. (7) at the heated surface temperature. For saturated FC-72 at atmospheric pressure and heater temperatures less than 20 °C above saturation, Eq. (7) predicts bubble departure diameters of 0.8 mm. Clearly, the most significant confinement effects are seen in the data of Figs. 6 and 7 for channel spacings below this value.

Not surprisingly, given the form of Eq. (7), many researchers have employed the Bond number to relate channel spacing to bubble departure diameter [7].

$$\mathrm{Bo} = \delta^2\left(\frac{g(\rho_f - \rho_g)}{\sigma_f}\right) \quad (8)$$

Subtle variations in the usage of this non-dimensional parameter grouping include the reciprocal of Eq. (8) [11], its square root [13,28], and the square root of the reciprocal [29], though occasionally it is based on the hydraulic diameter (2δ for a parallel-plate channel) instead of the channel spacing. Numerous researchers, including [11,13,28,29], identify $\mathrm{Bo}\approx 1$ (as defined above) as generally delineating the transition between confined and unconfined behaviors. The data shown in Figs. 6 and 7 support this notion as well, with channel spacings of 1.0 mm and 0.7 mm in saturated FC-72 equal to Bond numbers of 1.9 and 0.9, respectively.

Unfortunately, while Bond number is clearly a key parameter, the relative magnitude of enhancement effects and heat flux transition points between enhanced "low" flux and deteriorated "high" flux vary from study to study and can not be resolved with the Bond number alone or predicted, for example, as a par-

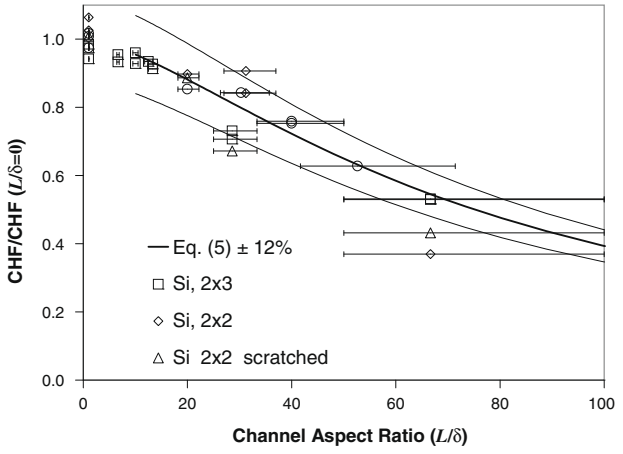

Fig. 9. Dependence of CHF data on channel aspect ratio, asymmetric heating.

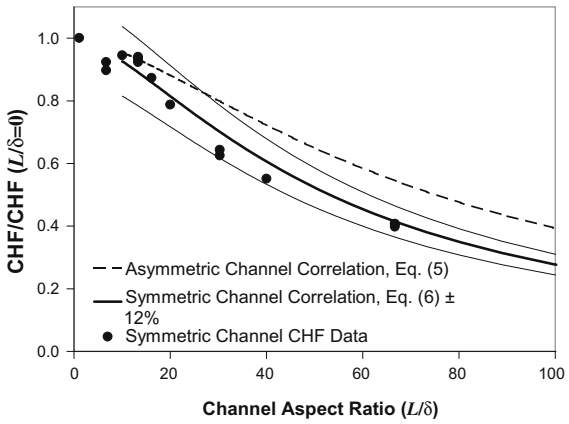

Fig. 10. Dependence of symmetric channel CHF data on aspect ratio.

ticular fraction of CHF [17]. While many researchers have correlated their own data (often a subset thereof) with theoretical models based on various assumed enhancement mechanisms (e.g. enhanced liquid convection [8], thin film evaporation [10]), no generally-applicable, unifying enhancement model has been achieved.

In the current study, the original EDM aluminum and polished silicon surfaces were modified in an attempt to bridge the performance gap between them. While, in general, rougher surfaces tend to exhibit higher boiling heat transfer rates, the slope of the roughened silicon boiling curve in Fig. 5 is quite different from the modified aluminum curves. This behavior demonstrates that a simple view of surface roughness (such as the Nishikawa surface roughness factor embedded in the Cooper pool boiling correlation) does not adequately describe the boiling-relevant features of surface microstructure. This fact is well established in the literature, e.g. [30]. Simple scratching of the polished silicon surface produces a narrow range of groove-like surface features, unlike the aluminum surfaces which contain a wide distribution of feature sizes and shapes, as shown in Fig. 4.

While the boiling curves of Fig. 5 show that scratching the polished silicon surface yields increased heat transfer rates in unconfined boiling, the relative magnitude of confinement-driven low flux enhancement was unaffected. That is, at a given channel spacing and heat flux, the fractional decrease in wall superheat relative to the unconfined pool boiling curves for the scratched and polished silicon surfaces was the same [17]. With the aluminum heaters, however, no reductions in wall superheat were observed, regardless of channel spacing and aluminum surface treatment. It is relatively unusual to publish studies showing a lack of expected enhancement. However, as explored in detail in [17], channel boiling experiments with methanol by Chien and Chen [14] and R-113 by Feroz and Kaminaga [31] also show a lack of expected confinement-driven enhancement at sub-unity Bond numbers on rough metal surfaces.

These observations tend to discount the potential importance or likelihood of proposed confinement-driven enhancement mechanisms unrelated to nucleation site characteristics. Evidence discounting enhanced liquid convection as the dominant mechanism in these experiments has also been provided through two phase computational fluid dynamics simulation in [32]. Alternatively, it is proposed that confined bubbles interact with and enhance the limited nucleation sites on the silicon surfaces in a manner that modifies bubble nucleation, growth, and departure, leading to increased heat transfer. This enhancement mechanism would not be available to the aluminum surfaces which are rich in nucleation sites with a wide distribution of characteristics.

Nucleation site interaction effects have been well documented in a wide variety of forms. Judd and Chopra [33], for example, studied the ability of growing or passing bubbles to deposit bubble embryos and initiate nucleation at adjacent sites. Chai et al. [34] theoretically considered additional effects of heat conduction in the boiling surface as well as thermodynamic aspects of bubble fluctuations on the stability of adjacent bubble nuclei. Bonjour et al. [35] investigated the effects of bubble coalescence on bubble growth and heat transfer from artificial nucleation sites with various separation distances and demonstrated that moderate coalescence increases heat transfer. Enhancement was attributed to vaporization of the relatively large supplementary microlayer formed between bubble stems. These insights reinforce the importance of investigating surface characteristics in addition to two phase flow phenomena in confined boiling systems and expose the fundamental drawbacks of representing microelectronic devices with rough metallic surfaces in direct liquid cooling experiments.

5.2. CHF trends

Unlike low flux nucleate boiling, confinement effects on CHF have been shown to be independent of surface material and roughness. The key parameter is the channel aspect ratio, L/δ, which determines the propensity of the increasing vapor fraction along the length of the channel to trigger premature dry out near the channel exit. The channel CHF correlations, Eqs. (5) and (6), also include the fluid to vapor density ratio and reduced pressure as parameters. As operating pressure (and reduced pressure) increases, the ratio of liquid density to vapor density will decrease. Interestingly, these effects counteract each other, and, as a result, the fluid density factor $(\rho_f/\rho_g)^{\psi}$ is relatively constant over the range of interest. This factor equals 22.3 for FC-72 at pressures of both 100 and 330 kPa and has a peak value of 23.4 at 200 kPa. However, it is important to note that while the relative effects of confinement on CHF will not vary significantly over this pressure range, pressure does have a significant impact on the baseline (unconfined) value. The CHF value for FC-72 increases by nearly 40% with increasing pressure up to a reduced pressure of 0.3, scaling with the pressure dependence of the fluid parameters in the Kutateladze–Zuber correlation, Eq. (2).

If one were to attempt predicting symmetric channel CHF using the asymmetric correlation, Eq. (5), and an "effective" channel spacing, the appropriate value would be expected to fall between well-defined upper and lower limits. Since at a given heat flux half as much vapor is generated in an asymmetric channel than a symmetric channel, the effective channel spacing used in the asymmetric correlation would have to be smaller than the actual symmetric channel spacing to capture the increased propensity for dry out. However, given the inevitable co-mingling of bubbles generated from each wall, the effective spacing would necessarily be greater than half the actual channel spacing, as it would not be appropriate to represent a symmetric channel with spacing δ as a simple combination of two asymmetric channels of spacing 0.5δ. Multiplying the aspect ratio in Eq. (5) by the square root of 2 to produce Eq. (6) is equivalent to assuming the effective spacing is 0.707δ. This choice is consistent with the practical limits identified above.

6. Conclusions

Experiments have been performed to expand the data available for saturated pool boiling CHF in narrow vertical channels, with particular emphasis on geometry, materials, and conditions applicable to passive, direct liquid cooling of microelectronics. Significant low flux nucleate boiling enhancement is shown to be achievable with bubble confinement, with mounting evidence pointing toward complex two phase flow and nucleation site interactions. At the upper limit of nucleate boiling, the relative effects of confinement on CHF are found to be independent of surface material and finish, and the deterioration in CHF is shown to be strongly dependent on channel aspect ratio. The Bonjour and Lallemand [12] correlation for asymmetrically heated channels has been found to accurately predict asymmetric channel CHF data obtained for FC-72. This correlation has been modified for symmetric channels, with a spacing-based correction, yielding good agreement with the data, particularly at smaller channel spacings where confinement effects are most significant. These results may be applied to the optimization and maximization of boiling heat transfer rates in confined geometries.

References

[1] A. Bar-Cohen, M. Arik, M. Ohadi, Direct liquid cooling of high flux micro and nano electronic components, Proc. IEEE 94 (8) (2006) 1549–1570.

[2] T. Guo, T. Zhu, Experimental research on the enhancement of boiling heat transfer of liquid helium in narrow channel, Cryogenics 37 (1997) 67–70.
[3] M. Kang, Pool boiling heat transfer in vertical annular crevices, Int. J. Heat Mass Transfer 45 (15) (2002) 3245–3249.
[4] A. Ulke, I. Goldberg, Flow regimes and heat transfer in vertical narrow annuli, in: Proceedings of the AIAA/ASME Thermophysics and Heat Transfer Conference HTD-129, ASME, New York, NY, 1990, pp. 81–89.
[5] S. Tieszen, V.S. Arpaci, S. Selamoglu, H. Merte Jr., Crevice boiling in steam generators, J. Heat Transfer 109 (3) (1987) 761–767.
[6] E. Ishibashi, K. Nishikawa, Saturated boiling heat transfer in narrow spaces, Int. J. Heat Mass Transfer 12 (1969) 863–894.
[7] M. Monde, H. Kusuda, H. Uehara, Critical heat flux during natural convective boiling in vertical rectangular channels submerged in saturated liquid, J. Heat Transfer Trans. ASME 104 (2) (1982) 300–303.
[8] A. Bar-Cohen, H. Schweitzer, Thermosyphon boiling in vertical channels, J. Heat Transfer Trans. ASME 107 (4) (1985) 772–778.
[9] Y. Fujita, H. Ohta, S. Uchida, Nucleate boiling heat transfer in vertical narrow space, in: Proceedings of the 1987 ASME/JSME Thermal Engineering Joint Conference, ASME, New York, NY, 1987, pp. 469–476.
[10] Y. Fujita, H. Ohta, S. Uchida, K. Nishikawa, Nucleate boiling heat transfer and critical heat flux in narrow space between rectangular surfaces, Int. J. Heat Mass Transfer 31 (2) (1988) 229–239.
[11] C. Xia, W. Hu, Z. Guo, Natural convective boiling in vertical rectangular narrow channels, Exp. Thermal Fluid Sci. 12 (3) (1996) 313–324.
[12] J. Bonjour, M. Lallemand, Effects of confinement and pressure on critical heat flux during natural convective boiling in vertical channels, Int. Commun. Heat Mass Transfer 24 (2) (1997) 191–200.
[13] J. Bonjour, M. Lallemand, Flow patterns during boiling in a narrow space between two vertical surfaces, Int. J. Multiphase Flow 24 (6) (1998) 947–960.
[14] L.H. Chien, C.L. Chen, An experimental study of boiling enhancement in a small boiler, in: Proceedings of the 34th National Heat Transfer Conference NHTC2000-12210, ASME, New York, NY, 2000, pp. 1–8.
[15] K.J.L. Geisler, A. Bar-Cohen, Optimization of pool boiling heat sinks including the effects of confinement in the interfin spaces, J. Electron. Packag. Trans. ASME 130 (4) (2008) 0410021–0410028.
[16] A. Bar-Cohen, K.J.L. Geisler, E. Rahim, Pool and flow boiling in narrow gaps—application to 3D chip stacks, in: Proceedings 5th European Thermal-Sciences Conference, Technische Universiteit, Eindhoven, 2008.
[17] K.J.L. Geisler, Buoyancy-Driven Two Phase Flow and Boiling Heat Transfer in Narrow Vertical Channels, Ph.D. thesis, University of Minnesota, Minneapolis, MN, 2007. Available from: <http://www.menet.umn.edu/~kgeisler/>.
[18] M.G. Cooper, Saturation nucleate pool boiling—a simple correlation, in: Proceedings of the 1st UK National Conference on Heat Transfer, Permagon Press, Elmsford, NY, 1984, pp. 785–793.
[19] K. Nishikawa, Y. Fujita, H. Ohta, S. Hidaka, Effects of system pressure and surface roughness on nucleate boiling heat transfer, Mem. Fac. Eng. Kyushu Univ. 42 (2) (1982) 95–123.
[20] N. Zuber, On the stability of boiling heat transfer, Trans. ASME 80 (1) (1958) 711–720.
[21] M. Arik, A. Bar-Cohen, Effusivity-based correlation of surface property effects in pool boiling CHF of dielectric liquids, Int. J. Heat Mass Transfer 46 (2003) 3755–3764.
[22] I. Mudawar, A.H. Howard, C.O. Gersey, An analytical model for near-saturated pool boiling critical heat flux on vertical surfaces, Int. J. Heat Mass Transfer 40 (10) (1997) 2327–2339.
[23] J.J. Ivey, D.J. Morris, Critical heat flux of saturation and subcooled pool boiling in water at atmospheric pressure, in: Proceedings of the International Heat Transfer Conference, 1966, pp. 129–142.
[24] V.K. Dhir, J.H. Lienhard, Hydrodynamic prediction of peak pool-boiling heat fluxes from finite bodies, ASME J. Heat Transfer 95 (2) (1973) 152–158.
[25] A. Watwe, A. Bar-Cohen, A. McNeil, Combined pressure and subcooling effects on pool boiling from a PPGA chip package, ASME J. Electronic Packaging 119 (2) (1997) 95–105.
[26] W. Tong, A. Bar-Cohen, T.W. Simon, Thermal transport mechanisms in nucleate pool boiling of highly-wetting liquids, in: Proceedings of the Ninth International Heat Transfer Conference, Hemisphere, New York, NY, 1990, pp. 27–32.
[27] R. Cole, W.M. Rohsenow, Correlation of bubble departure diameters for boiling of saturated liquids, AIChE Chem. Eng. Prog. Symp. Ser. 65 (1969) 211–213.
[28] S. Yao, Y. Chang, Pool boiling heat transfer in a confined space, Int. J. Heat Transfer 26 (6) (1983) 841–848.
[29] P.A. Kew, K. Cornwell, Correlations for the prediction of boiling heat transfer in small-diameter channels, Appl. Thermal Eng. 17 (8–10) (1997) 705–715.
[30] I.L. Pioro, W. Rohsenow, S.S. Doerffer, Nucleate pool-boiling heat transfer. I: review of parametric effects of boiling surface, Int. J. Heat Mass Transfer 47 (23) (2004) 5033–5044.
[31] C. Feroz MD., F. Kaminaga, Boiling heat transfer characteristics of R-113 in a vertical small diameter tube under natural circulation condition, Int. J. Heat Mass Transfer 45 (24) (2002) 4823–4829.
[32] K.J.L. Geisler, A. Bar-Cohen, Numerical and experimental investigations of boiling enhancement in buoyancy-driven microchannels, in: Proceedings of the Eleventh Intersociety Conference on Thermal and Thermomechanical Phenomena in Electronic Systems, IEEE, Piscataway, NJ, 2008, pp. 65–74.
[33] R.L. Judd, A. Chopra, Interaction of the nucleation processes occurring at adjacent nucleation sites, J. Heat Transfer 115 (4) (1993) 955–962.
[34] L.H. Chai, X.F. Peng, B.X. Wang, Nucleation site interaction during boiling, Int. J. Heat Mass Transfer 43 (23) (2000) 4249–4258.
[35] J. Bonjour, M. Clausse, M. Lallemand, Experimental study of the coalescence phenomenon during nucleate pool boiling, Exp. Thermal Fluid Sci. 20 (3) (2000) 180–187.